Grain Structures and Boundaries on Microcrystalline Copper Covered with an Octadecanethiol Monolayer Revealed by Sum Frequency Generation Microscopy

ARTICLE *in* JOURNAL OF PHYSICAL CHEMISTRY LETTERS · APRIL 2015

Impact Factor: 7.46 · DOI: 10.1021/acs.jpclett.5b00215

2 AUTHORS, INCLUDING:

Ming Fang
University of Houston
3 PUBLICATIONS **4** CITATIONS

THE JOURNAL OF PHYSICAL CHEMISTRY Letters

Letter

pubs.acs.org/JPCL

Grain Structures and Boundaries on Microcrystalline Copper Covered with an Octadecanethiol Monolayer Revealed by Sum Frequency Generation Microscopy

Ming Fang and Steven Baldelli*

Department of Chemistry, University of Houston, 4800 Calhoun Road, Houston, Texas 77204-5003, United States

Supporting Information

ABSTRACT: An octadecanethiol (ODT) self-assembled monolayer on microcrystalline copper was investigated by sum frequency generation (SFG) imaging microscopy. The crystal grain and grain boundaries of the copper surface were mapped in the SFG image based on the strong brightness contrast of the SFG signal across the boundary. Local SFG spectra reveal significant difference with each other as well as the average SFG spectra, indicating the heterogeneity of the copper surface resulting from copper grains with distinct crystallographic facets and orientations. It is demonstrated that the SFG signal of crystalline domain areas contains azimuthal anisotropy with respect to the plane of incidence. In addition, the statistical orientation analyses of amplitude ratio of CH_3-sym/CH_3-asym and corresponding contour maps imply that the orientation of ODT molecules is affected by the underlying copper.

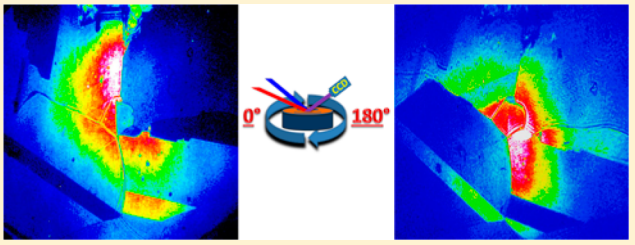

The mechanism of metallic corrosion and inhibition has been the subject of a vast amount of research due to its significance to the modern world.[1] Previous corrosion studies have often been performed on the macroscopic scale, but corrosion behavior also strongly depends on microscopic features, that is, crystal grains with different crystallographic orientations, which exist on most polycrystalline metallic surfaces.[2,3] Recent studies demonstrated that the pattern differences across microscopic crystal grains and grain boundaries (GBs) induce the localized corrosion on the copper surface.[4−6] Features such as surface current difference across grains,[7,8] extensive misorientation between grains,[9] and grain sizes[10,11] contribute to heterogeneous corrosion occurring on the surfaces. Because of the existence of heterogeneous corrosion on the micrometer scale, understanding the role of crystallographic orientation to local corrosion process is a worthwhile goal. Therefore, high-resolution imaging techniques are necessary. There have been numerous studies reported to investigate the role of crystallographic orientation and GBs on metal corrosion occurring in the initial stages, including studies performed using electron backscattering diffraction (EBSD),[3] atomic force microscopy (AFM),[3] and scanning tunneling microscopy (STM),[5] which are able to provide highly accurate topographic information on surface and structure of the corrosion site. Under some circumstance, scanning probe microscopy such as AFM and STM could deduce the surface molecular functional group and packing geometry with atomic resolution;[12−17] however, local chemical information obtained from vibrational spectroscopy of molecular functionality on the surface, which is important to interpret and understand local copper corrosion and inhibition behaviors, is still lacking.

Alkanethiol self-assembled monolayers (SAMs) on metal surfaces have been extensively studied due to their identical surface chemical functionality, excellent stability, and wide application such as improving corrosion resistance for copper surfaces.[18−22] One popular technique for studying the alkanethiol monolayer on the surface at a molecular level is sum frequency generation vibrational spectroscopy (SFG-VS), which has excellent chemical selectivity and interfacial sensitivity. Previous SFG-VS studies have been applied to characterize the ordered monolayer of alkanethiols formed on copper surfaces.[23] Recently, Hosseinpour et al. employed SFG-VS to monitor the oxidation of ODT-covered copper in dry air and observed the formation of a thin layer of copper(I) oxide beneath the ODT monolayer based on the phase change of SFG spectra.[19] In addition, they also applied SFG-VS to study the chain length effect of alkanethiols by analyzing corrosion behaviors induced by formic acid on copper and found the inhibition ability increasing continuously with chain length; however, these SFG studies focused on average spectral analysis without providing any local information about the surface. In recent studies, the SFG imaging technique that combines SFG-VS with a microscope probe demonstrated high spatial resolution combined with SFG local spectra to study monolayers on a heterogeneous metal surface.[24−26] Santos et al. performed SFG imaging to study localized corrosion processes occurring on copper surfaces in an oxygenated environment by monitoring Cu_2O formation;[24] however, the important metallic features including the crystal grains and GBs

Received: January 31, 2015
Accepted: April 1, 2015

DOI: 10.1021/acs.jpclett.5b00215
J. Phys. Chem. Lett. 2015, 6, 1454−1460

have not been observed and interpreted by the SFG imaging technique.

It has been proven that micrometer-sized crystal grains and GB structures form on copper surfaces when annealed at high temperature in a hydrogen atmosphere.[27] In this study, SFG imaging was used to investigate ODT monolayers on this type of copper surface. Micrometer-sized copper grains and GBs were clearly observed in the SFG image. Compared with traditional diffraction tools used for the crystallographic research, the SFG technique that offers several unique features, including noninvasivity and versus bulk surface selectivity, has already been developed for probing various crystal surfaces.[28] Characteristic anisotropy of the SFG signal response in each grain suggests that SFG performed in microscopy mode shows high promise for imaging the local metal surface symmetry with high spatial resolution. In addition, the corresponding local spectra demonstrate the advantage of SFG imaging in providing sufficient molecular information on heterogeneous metal surfaces. As a result, it shows the promising application for the research of corrosion behavior on microcrystalline metal surfaces.

A theoretical review of SFG spectroscopy is briefly presented here. SFG is a second-order nonlinear optical process in which a tunable infrared beam is spatially and temporally overlapped with a 1064 nm beam on the surface to generate a SFG output.[29] The second-order polarization as shown in eq 1 is the source term for the radiation of the SFG signal. The SFG signal is emitted at a specific angle based on the conservation of momentum. SFG is a highly surface-sensitive technique because the SFG process is forbidden in a bulk medium with inversion symmetry under the electric dipole approximation.[30]

$$I_{SF} \propto |P_{SF}^{(2)}|^2 \propto |\chi_{eff}^{(2)}|^2 I_{1064nm} I_{IR} \quad (1)$$

As shown in eq 2, the second-order susceptibility tensor $\chi_{eff}^{(2)}$, which is described as the sum of a nonresonant part $\chi_{NR}^{(2)}$ and resonant part $\chi_{R}^{(2)}$, relates the induced second-order polarization response to the incident light intensity. $\chi_{NR}^{(2)}$ is the nonresonant contribution typically attributed to electronic excitation of substrate and the adsorbate. $\chi_{R}^{(2)}$ is associated with vibrational modes of the adsorbate layer. When the frequency of an incident infrared beam (ω_{IR}) is resonant with a surface vibrational mode, q, the $\chi_{R}^{(2)}$ is changed as well as the SFG intensity. The $\chi_{eff}^{(2)}$ is related to molecular hyperpolarizability $\beta^{(2)}$ through ensemble average over all possible molecular orientations shown in eq 2. The molecular orientation including tilt angle (θ), azimuth angle (in surface coordinate system) (φ), and rotation angle (ψ) are defined in Figure 1. The sample azimuth angle (in the laboratory coordinate system) that is important in this study is also demonstrated in Figure 1. N, A_q, ω_{IR}, ω_q, and Γ_q are the surface molecular density, amplitude, frequency of the IR beam, resonant frequency, and the damping constant of the qth vibrational mode, respectively. Equation 2 is the basis equation for the nonlinear model fitting of SFG spectra used for orientation analysis and mapping results.

$$\chi_{eff}^{(2)} = \chi_{R}^{(2)} + \chi_{NR}^{(2)} = \sum_q \frac{A_q}{\omega_q - \omega_{IR} - i\Gamma_q} + A_{NR} e^{i\phi} \quad (2)$$

Both $\chi_{R}^{(2)}$ and $\chi_{NR}^{(2)}$ are complex quantities, so the SFG spectra are complicated by the interference term shown in eq 3, especially for the metal that contributes strong nonresonant

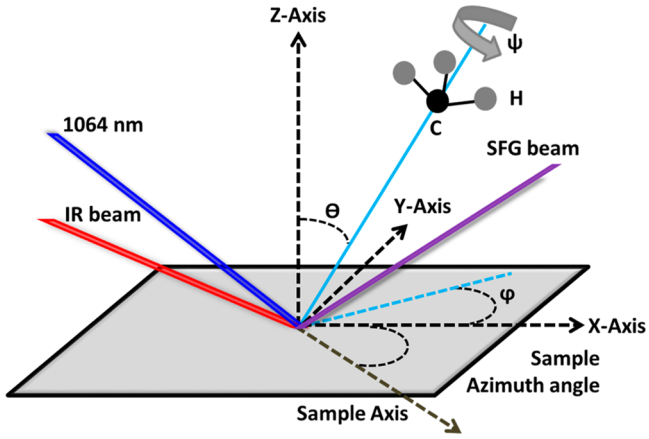

Figure 1. Definition of the tilt angle (θ), azimuth angle (φ), and rotation angle (ψ) of molecular adsorbed on the surface and sample azimuth angle.

background due to the nearly free electrons in surface region, resulting in complex line shapes.[31,32] The ε and δ denote the phase of $\chi_{R}^{(2)}$ and $\chi_{NR}^{(2)}$, and the phase difference of $\chi_{R}^{(2)}$ and $\chi_{NR}^{(2)}$ is relative nonresonant phase ϕ.

$$I_{SF} \propto |\chi_{eff}^{(2)}|^2 = ||\chi_{NR}^{(2)}|e^{i\varepsilon} + |\chi_{R}^{(2)}|e^{i\delta(\omega_{IR})}|^2 = |\chi_{NR}^{(2)}|^2 + |\chi_{R}^{(2)}|^2 + 2|\chi_{NR}^{(2)}||\chi_{R}^{(2)}| \cos[\varepsilon - \delta] \quad (3)$$

The material used in this work was a polycrystalline rectangular copper sheet (Goodfellow, 99.99%) with an area of 1 cm^2 and thickness of 3 mm. One side of copper surface was polished down to 0.1 μm by diamond paste. The copper was annealed in furnace with argon (300 sccm) and hydrogen (30 sccm) at temperature of 1050 °C for 3 h. Then, the copper sample was cooled to room temperature in argon and hydrogen flow atmosphere and was immediately immersed into 5 mM ODT/ethanol solution. After 2 h, the copper sample was taken out from the ODT solution, rinsed with ethanol, and dried under nitrogen flow in the glovebox to prevent the oxidation of copper. The copper was then mounted in the SFG cell filled with nitrogen gas. The SFG cell was mounted on an x-y-z plus tip/tilt 5 axis stage for the SFG imaging experiment.

SFG imaging microscopy has been described in detail elsewhere.[25] A picosecond pulsed Nd:YAG laser (EKSPLA) with a 20 Hz repetition rate provides the 1064 nm beam that pumps the optical parametric generator/amplifier(OPG/OPA) to yield the IR beam that is tunable from 2000 to 4000 cm^{-1}. The incidence angles of the IR and 1064 pump beams are 70 and 60° from the surface normal, respectively. The emitted angle of SFG beams is 62.1° from surface normal. The polarizations of the two incident beams are both p-polarized (parallel to the incidence plane) set by polarizer, and the polarization of the SFG signal is considered to be p-polarized (p-polarized SFG signal dominates the SFG signal), and this polarization combination is designated as PPP. A Roper Scientific CCD camera with 1024 × 1024 pixel array was used for SFG beam profile collection. Each SFG image is 1024 × 1024 pixels, and 1 pixel is corresponding to 1 μm distance on surface. The spatial resolution is ~2 μm. The SFG beam wavelength (IR wavenumber range 2750 cm^{-1}-3050 cm^{-1}) is ~808 nm. An 808 nm unpolarized CW laser with a wavelength that is close to the SFG wavelength at an incidence angle of 62.1° is used to simulate the SFG beam path and generates a

DOI: 10.1021/acs.jpclett.5b00215
J. Phys. Chem. Lett. 2015, 6, 1454−1460

reference image that shares the same sample position with the SFG image.

Figure 2a,c presents the optical image using 808 nm optical microscope on the copper sample at two azimuth angles of 0

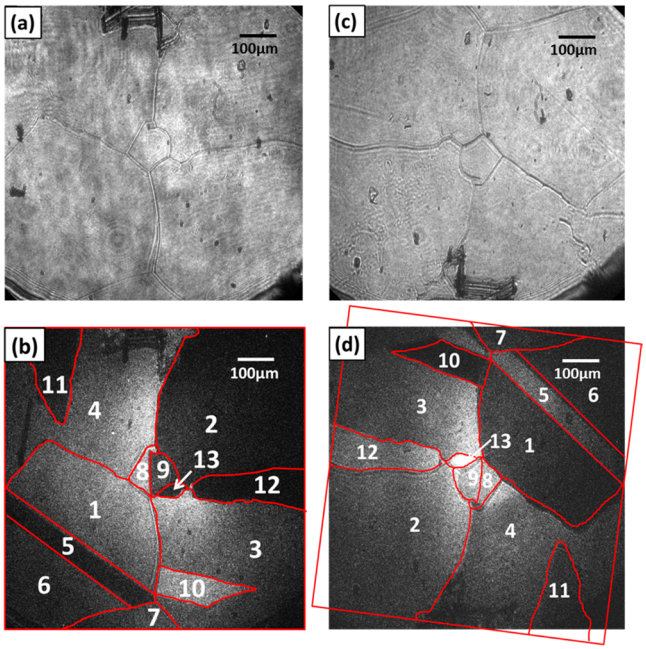

Figure 2. Left (a,b): Optical image (wavelength, 808 nm) and unprocessed SFG image (IR wavenumber: 3050 cm^{-1}) of the copper surface with the ODT monolayer at the azimuth angle of 0°. Right (c,d): Optical image (wavelength, 808 nm) and unprocessed SFG image (IR wavenumber: 3050 cm^{-1}) of the copper surface with the ODT monolayer at the azimuth angle of 180°. SFG images are taken with the PPP polarization. The red frame marked the GBs in panel c and was rotated to fit the GBs in panel d.

and 180°, respectively. Several domains and boundaries are displayed in the optical images. The domain sizes are a few hundred micrometers. The whole copper surface is optically flat, and different domains show no brightness contrast with each other. When the sample's azimuth angle changes, the contrast in the optical image is essentially unchanged.

Figure 2b,d shows the SFG image for the two azimuth angles at 3050 cm^{-1}. These images are slices from the 51 image stack acquisition from 2800 to 3050 cm^{-1}. Because the image was acquired in the nonresonant IR region (3050 cm^{-1}), the SFG intensity in Figure 2b,d is associated with the nonlinear susceptibility of the copper substrate. On the basis of the observation, several domains with distinctive brightness contrast were identified in the SFG image with various sizes (10−300 μm), suggesting difference of SFG signal response existing in each domain, which was not detected in the corresponding optical images. EBSD techniques have been applied to characterize copper surfaces, which are obtained using the same sample preparation procedure, and the crystallographically diversified Cu surface was identified with various crystal facets such as Cu(111), Cu(310), and Cu(410).[2,27] Compared with the domains shown in the EBSD image, the domains of the SFG image were similar in size and shape. Thus, the domain structure in the SFG image could also be explained in terms of micrometer-sized crystal facets existing on the copper surface. Because the SFG intensity is directly associated with the nonlinear susceptibility of the copper substrate, the SFG intensity difference in different domains of the image is related to the nonlinear surface susceptibility varying on different crystal grains of the copper surface.

Next, the spatial correlation of the optical image with the SFG image was investigated. All boundaries shown in the optical image are observed in the SFG image; however, some clearly observable boundaries in the SFG image were not obtained in the optical image, such as the boundary between domains 1 and 5 in Figure 2c. Previous studies showed that when the collision of the formed domains after the initiation of atom nucleation occurs on the copper surface, the extent of misorientation of the surface atom structures in two adjacent grain domains determines the formation of boundaries with clear geometrical boundaries.[9] The reflectivity difference resulting from the geometry makes the boundaries appear in the optical image. In other words, the boundaries between crystal grains without remarkable boundary grooves could not be distinguished in the optical image. Hence, the SFG microscope is able to reveal crystal grain structure of metal surface.

In a comparison between Figures 2b and 2d, the brightness contrast between each domain changes while the sample is rotated around the surface normal. For example, domain 1 is brighter than domain 2 in Figure 2b, while the domain 2 is brighter than domain 1 in Figure 2d. In addition, some GBs that are obvious in Figure 2b disappear in Figure 2d, such as that between regions 11 and 4 in Figure 2a. In contrast, some domains such as 7, 12, and 13 that are obvious in Figure 2d are not perceivable in Figure 2c. A series of SFG images with four more azimuth angles presented in Figure S3 in the SI confirm this phenomenon. These results imply that there is azimuthal anisotropy of the SFG response in copper domains. On the basis of previous studies performed by nonlinear optical techniques including second harmonic generation (SHG) and SFG-VS on gold,[33] silver[34] and copper,[35] these effects are correlated to the azimuthal anisotropy of the nonlinear susceptibility of metallic crystal facets. A phenomenological macroscopic explanation on the anisotropy of nonlinear optical signal response of single crystal facets such as (111), (110), and (100) was reported in the results of Sipe and coworkers.[36] On the basis of this discussion and the previous studies, the brightness contrast of the different domains results from various crystal facets that exist on the copper surface.

A series of SFG spectra of the ODT monolayer on the copper surface were extracted from the set of SFG images for azimuth angles from 0 and 180° and presented in Figure 3. The five peaks of the SFG spectra corresponding to the CH_2 symmetric stretch 2850 cm^{-1}, the CH_3 symmetric stretch 2880 cm^{-1}, the CH_2 Fermi resonance 2915 cm^{-1}, the CH_3 Fermi resonance 2940 cm^{-1}, and the CH_3 asymmetric stretch 2970 cm^{-1}, respectively, were observed.[37] Shown in Figure 3a,d are the average SFG spectra of the sample at two different azimuth angles, revealing minor difference between each other; however, the line shapes of the local spectra in Figure 3b,c show remarkable differences from each other as well as the average spectrum in Figure 3a, respectively. The line shape of the SFG spectrum depends on the relative phase ϕ between $\chi_R^{(2)}$ and $\chi_{NR}^{(2)}$, as shown in eq 2. The electronic structure of the metal substrates can cause the nonresonant background and relative phase change.[32] Thus, the spectral changes observed in Figure 3 could be explained in terms of electronic structure difference resulting from two aspects: different crystal facets on copper

DOI: 10.1021/acs.jpclett.5b00215
J. Phys. Chem. Lett. 2015, 6, 1454−1460

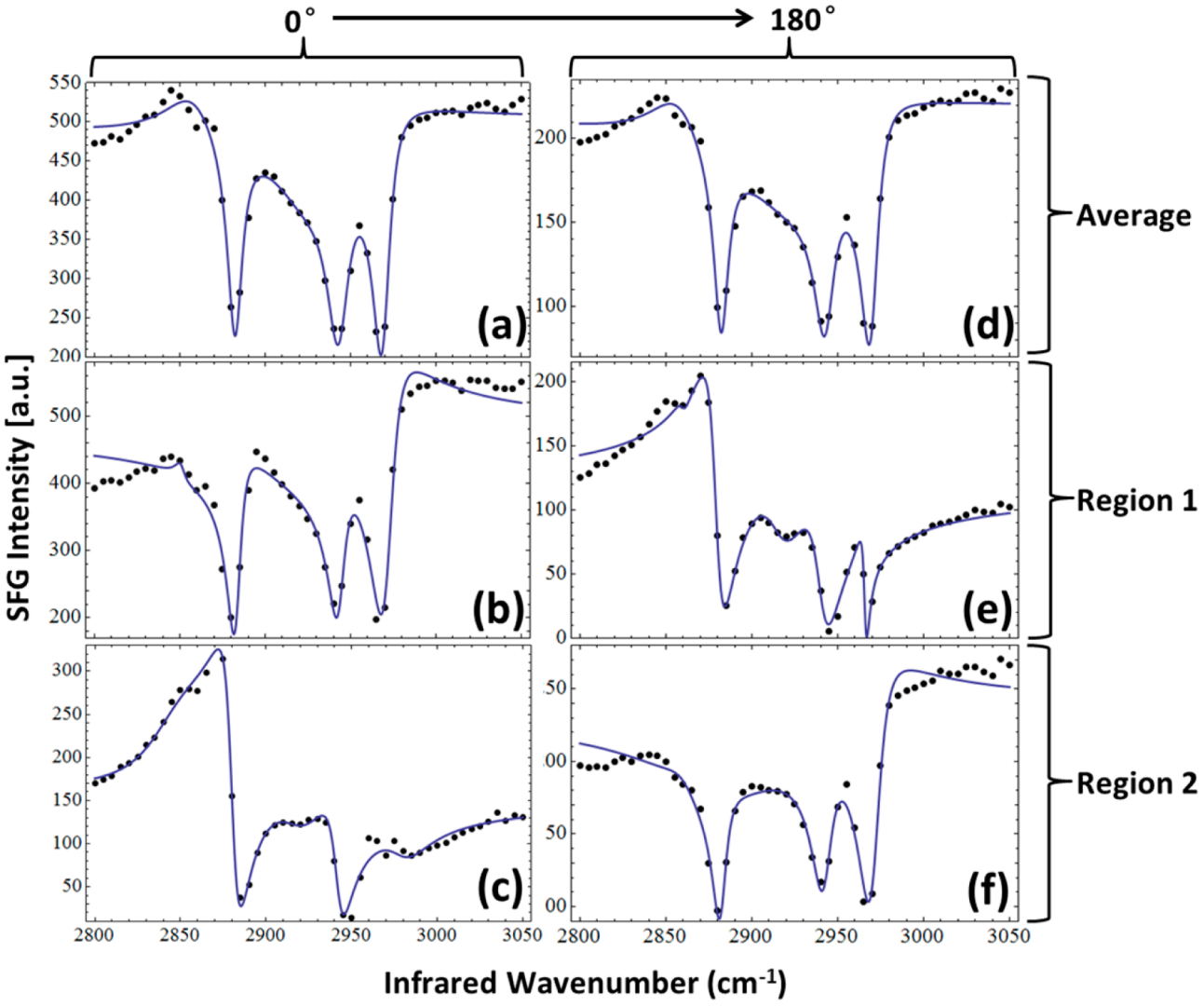

Figure 3. SFG spectra (2800−3050 cm^{-1}) of the copper surface with an ODT self-assembled monolayer. (a,d) Average SFG spectra of Figures 2b and 2d, respectively. (b,c) SFG spectra from domain 1 and domain 2 in Figure 2b, respectively. (e,f) SFG spectra from domains 1 and 2 in Figure 2d, respectively. The solid blue lines are the fits using eq 2. The fitting results are listed in Table 1 of the Supporting Information.

surface and same crystal facet with different orientations of ODT. This also implies that the SFG relative phase and nonresonant background are coupled to the underlying copper crystal structure.

Both of the SFG spectra in Figure 3b,e are obtained from the same sample area, which is domain 1. Nevertheless, comparing the spectra, the spectral line shapes show remarkable difference. This is also applied to the comparison of spectra in Figure 3c,f. These results indicate that SFG spectra exhibit an obvious anisotropy while the sample azimuth angle changes. From Table 1 in the SI, the nonresonant part such as relative phase and resonant part such as the amplitude of $CH_{3\text{-sym}}$ change values with respect to azimuthal rotation. The nonresonant SFG signal is generated from the copper substrate, and its dependence on azimuth angle is interpreted in the following context. The nonresonant parameters such as the relative phase of SFG spectra result from the anisotropy of the nonlinear susceptibility of crystalline substrate. This type of anisotropy of the nonlinear susceptibility was also observed in previous SFG studies on Au(111)[33] and Si(111).[38] The resonant part of SFG signal is generated at the air/monolayer interface, and its dependence on azimuth angle is directly related to the monolayer orientation. Therefore, a qualitative analysis for our results denotes an orientation distribution for the ODT chains that exhibit narrow angular ranges in azimuth angles. Similar ordered monolayer systems on the poly(vinyl alcohol) surface[39] and the LB film surface of cadmium arachidate[40] also show anisotropy of SFG signals.

The remarkable difference between the local spectra with average spectra as well as the spectral anisotropy shown in Figure 3 is of great importance because many SFG studies were performed on monolayers absorbed on various metallic surfaces. Without independent knowledge of various crystal grains existing on the metal surface, the ensemble average information on such surface is usually obtained by a wholesale integration of spectrum based on the assumption that surface crystal facet distribution is spatially homogeneous. However, the local features on individual grains, and especially the GBs, might be overlooked, which leads to an inaccurate interpretation of the system. Hence, analyzing the local spectrum in more detail is indispensable. The ability to visualize the surface by SFG imaging provides new perspective for the understanding of surface chemistry on metals on the micrometer scale.

DOI: 10.1021/acs.jpclett.5b00215
J. Phys. Chem. Lett. 2015, 6, 1454−1460

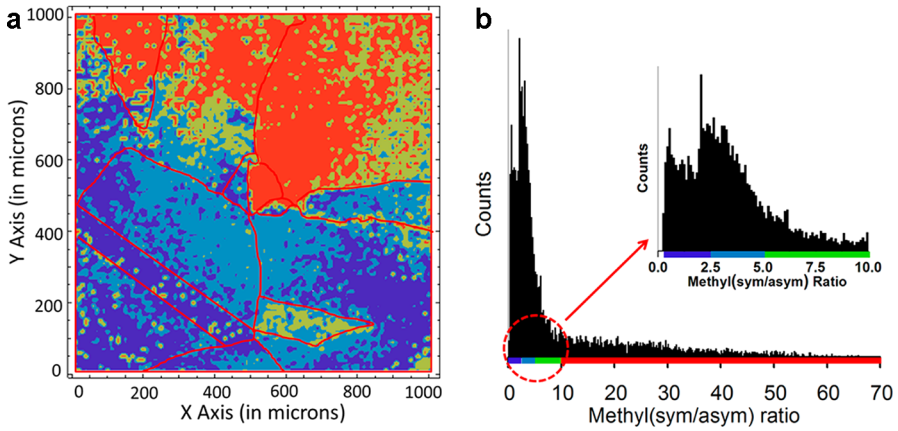

Figure 4. (a) Contour map of amplitude ratio of $CH_{3\text{-sym}}/CH_{3\text{-asym}}$. (b) Histogram of amplitude ratio of $CH_{3\text{-sym}}/CH_{3\text{-asym}}$. Corresponding colors (blue: 0−2.5, light blue: 2.5−5, green: 5−10, red: 10−70) in the contour map (panel a) represent specific amplitude ratio range selected in the histogram (panel b). The red color marks the corresponding area in the selected ratio range.

The whole set of SFG image (azimuth angle 0° shown in Figure 2b) was divided into 10 000 regions of interest (ROI), which is a 10 μm × 10 μm square. The SFG spectra were extracted and fitted by eq 2. The amplitude ratios of methyl symmetric stretching mode and methyl asymmetric stretching mode of each ROI were obtained and then used to reconstruct a chemical image and presented in Figure 4.

The methyl group of ODT has two fundamentals in the CH stretch region. On the basis of the surface IR selection rule on perfect conductor, only the fundamentals that have a nonzero component of transition moment positioned along the surface normal are observed in the SFG spectrum. When the C_3 axis of the methyl group tilts farther away from the surface normal, the asymmetric mode becomes greater and the symmetric mode becomes smaller.[41,42] The SFG technique is able to analyze the orientation conformation of the terminal methyl group of ODT (including the tilt angle, azimuth angle, and rotation angle demonstrated in Figure 1) on copper surface based on the amplitude ratio of $CH_{3\text{-sym}}/CH_{3\text{-asym}}$ under PPP polarization combination.[40,43] Parameters such as the interfacial refractive indices, as well as the molecular hyperpolarizability elements and relative phase, are required to perform a comprehensive calculation of orientation, and this analysis is ongoing. In this study, the contour map of the amplitude ratio of $CH_{3\text{-sym}}/CH_{3\text{-asym}}$ shown in Figure 4a is spatially correlated to the local orientation angle of ODT molecules on the copper surface. The monolayer heterogeneity could be deduced from the amplitude ratio analysis. In Figure 4a, several domains and boundaries, of which the size and shape are similar to the domains in Figure 2b, are observed. The red frame of Figure 2b is applied on Figure 4a, which makes this effect more obvious. It illustrates that the packing of ODT molecules on copper surface is heterogeneous and the heterogeneity of molecular packing is resulting from copper substrates with various grain structures underneath the ODT monolayer.

Figure 4b shows the amplitude ratio distribution from 0 to 70.0. Most ROI ratios are located between 0 to 10, and this range in the histogram is magnified in Figure 4b. The domains that are marked with four different colors shown in Figure 4a correspond to the four ratio ranges, which are selected to magnify the domain effect shown in Figure 4a (0−2.5, 2.5−5, 5−10, and 10−70), respectively. It suggests that each crystal grain contains its characteristic SAMs monolayer packing behavior, which is different from other crystal grains, and this is well known from previous studies.[44,45] The reason why the underlying grain structure affects the top monolayer packing behavior could be that the copper surface atom density and electron density vary with different copper grains, which makes ODT molecules more preferentially be adsorbed on the grain with special facet, thereby forming domains following the underlying copper grain structure. It further suggests that the surface becomes more heterogeneous with the existence of the copper grain structure.

On the basis of the assumption that the tilt angle distribution for the ODT molecules follows a δ function and the rotation angle together with azimuth angle are randomly distributed, a theoretical curve simulating the amplitude ratio of $CH_{3\text{-sym}}/CH_{3\text{-asym}}$ as a function of the tilt angle of methyl groups was plotted and is presented in the Figure S4 in the SI. (More detail about this theoretical curve is presented in the SI.) However, crystallographic domains of the copper substrate should give rise to various azimuthal ODT packing domains. Such domains have already been identified by STM in alkanethiol SAMs on Au (111).[46,47] It has to be pointed out that the assumption that the azimuth angles are random distribution introduces bias to calculation. More systematic research and discussion for azimuth angle distribution should be performed for accurate determination of the orientation of the ODT monolayer in such a system. Besides, Fresnel factors that relate the electric field in bulk media to the electric field at the interface are normally calculated using the equations given by Zhuang et al.[48] based on the assumption that the substrates are homogeneous; however, the atom density and crystal orientation with respect to incident light vary on crystal grains, which complicate Fresnel factors. Thus, for the SFG orientation analysis on similar systems, this effect should be discussed in more detail in the future.

In summary, micrometer-scale crystal grains and GBs were identified by the SFG imaging technique for the first time. It provides new clues for a broad range of interest such as localized corrosion processes on copper surfaces with crystal grain structures. Besides, the marked difference of SFG spectra across domains relates the localized molecular information to the overall performance of the whole surface area, which suggests the importance of considering the heterogeneity of ODT monolayers on polycrystalline copper surfaces. Consequently, spectroscopic visualization of the surface leads to an accurate understanding of surface chemistry. The anisotropy of

DOI: 10.1021/acs.jpclett.5b00215
J. Phys. Chem. Lett. 2015, 6, 1454−1460

SFG spectra observed in the present work will inspire the further SFG research on the metal substrates.

■ ASSOCIATED CONTENT

Supporting Information

Additional experimental information including schematic diagram of SFG imaging setup, fitting results of SFG spectra, and SFG images in six azimuth angles and orientation simulation curve. This material is available free of charge via the Internet at http://pubs.acs.org.

■ AUTHOR INFORMATION

Corresponding Author

*E-mail: sbaldelli@uh.edu.

Notes

The authors declare no competing financial interest.

■ ACKNOWLEDGMENTS

We gratefully acknowledge the National Science Foundation (CHE1361885) for providing generous support for this project. We thank Professor Jiming Bao and Kamrul Alam (University of Houston) for preparing samples. We also appreciate valuable discussions with Desheng Zheng and Qiongzheng Hu (University of Houston) and Michael Donovan (Max Planck Institute for Polymer Research). We thank Joon Hee Jang (University of Houston) for developing the curve-fitting program and Professor Yang Ding-Shyue and Xin He (University of Houston) for the electron diffraction results and valuable suggestion.

■ REFERENCES

(1) Schweitzer, P. A. *Fundamentals of Corrosion: Mechanisms, Causes, and Preventative Methods*; CRC Press: Boca Raton, FL, 2010.

(2) Martinez-Lombardia, E.; Maurice, V.; Lapeire, L.; De Graeve, I.; Verbeken, K.; Kestens, L.; Marcus, P.; Terryn, H. In Situ Scanning Tunneling Microscopy Study of Grain-Dependent Corrosion on Microcrystalline Copper. *J. Phys. Chem. C* **2014**, *118*, 25421−25428.

(3) Lapeire, L.; Martinez Lombardia, E.; Verbeken, K.; De Graeve, I.; Kestens, L. A. I.; Terryn, H. Effect of Neighboring Grains on the Microscopic Corrosion Behavior of a Grain in Polycrystalline Copper. *Corros. Sci.* **2013**, *67*, 179−183.

(4) Park, C. J.; Lohrengel, M. M.; Hamelmann, T.; Pilaski, M.; Kwon, H. S. Grain-Dependent Passivation of Surfaces of Polycrystalline Zinc. *Electrochim. Acta* **2002**, *47*, 3395−3399.

(5) Martinez-Lombardia, E.; Lapeire, L.; Maurice, V.; De Graeve, I.; Verbeken, K.; Klein, L. H.; Kestens, L. A. I.; Marcus, P.; Terryn, H. In Situ Scanning Tunneling Microscopy Study of the Intergranular Corrosion of Copper. *Electrochem. Commun.* **2014**, *41*, 1−4.

(6) Martinez-Lombardia, E.; Gonzalez-Garcia, Y.; Lapeire, L.; De Graeve, I.; Verbeken, K.; Kestens, L.; Mol, J. M. C.; Terryn, H. Scanning Electrochemical Microscopy to Study the Effect of Crystallographic Orientation on the Electrochemical Activity of Pure Copper. *Electrochim. Acta* **2014**, *116*, 89−96.

(7) Schreiber, A.; Schultze, J. W.; Lohrengel, M. M.; Karman, F.; Kalman, E. Grain Dependent Electrochemical Investigations on Pure Iron in Acetate Buffer pH 6.0. *Electrochim. Acta* **2006**, *51*, 2625−2630.

(8) Lill, K. A.; Hassel, A. W.; Frommeyer, G.; Stratmann, M. Scanning Droplet Cell Investigations on Single Grains of a FeAlCr Light Weight Ferritic Steel. *Electrochim. Acta* **2005**, *51*, 978−983.

(9) Miyamoto, H.; Yoshimura, K.; Mimaki, T.; Yamashita, M. Behavior of Intergranular Corrosion of <011> Tilt Grain Boundaries of Pure Copper Bicrystals. *Corros. Sci.* **2002**, *44*, 1835−1846.

(10) Luo, W.; Xu, Y.; Wang, Q.; Shi, P.; Yan, M. Effect of Grain Size on Corrosion of Nanocrystalline Copper in NaOH Solution. *Corros. Sci.* **2010**, *52*, 3509−3513.

(11) Ralston, K. D.; Birbilis, N. Effect of Grain Size on Corrosion: A Review. *Corrosion* **2010**, *66*.

(12) Claypool, C. L.; Faglioni, F.; Goddard, W. A.; Gray, H. B.; Lewis, N. S.; Marcus, R. Source of Image Contrast in STM Images of Functionalized Alkanes on Graphite: A Systematic Functional Group Approach. *J. Phys. Chem. B* **1997**, *101*, 5978−5995.

(13) Claypool, C. L.; Faglioni, F.; Goddard, W. A.; Lewis, N. S. Tunneling Mechanism Implications from an STM Study of H3C-(CH2)(15)HC=C=CH(CH2)(15)CH3 on Graphite and C14H29OH on MoS2. *J. Phys. Chem. B* **1999**, *103*, 7077−7080.

(14) Claypool, C. L.; Faglioni, F.; Matzger, A. J.; Goddard, W. A.; Lewis, N. S. Effects of Molecular Geometry on the STM Image Contrast of Methyl-and Bromo-Substituted Alkanes and Alkanols on Graphite. *J. Phys. Chem. B* **1999**, *103*, 9690−9699.

(15) Yu, H.; Webb, L. J.; Ries, R. S.; Solares, S. D.; Goddard, W. A.; Heath, J. R.; Lewis, N. S. Low-temperature STM Images of Methyl-terminated Si (111) Surfaces. *J. Phys. Chem. B* **2005**, *109*, 671−674.

(16) Barrena, E.; Kopta, S.; Ogletree, D. F.; Charych, D. H.; Salmeron, M. Relationship between Friction and Molecular Structure: Alkylsilane Lubricant Films under Pressure. *Phys. Rev. Lett.* **1999**, *82*, 2880−2883.

(17) Barrena, E.; Ocal, C.; Salmeron, M. Molecular Packing Changes of Alkanethiols Monolayers on Au (111) under Applied Pressure. *J. Chem. Phys.* **2000**, *113*, 2413−2418.

(18) Hosseinpour, S.; Johnson, C. M.; Leygraf, C. Alkanethiols as Inhibitors for the Atmospheric Corrosion of Copper Induced by Formic Acid: Effect of Chain Length. *J. Electrochem. Soc.* **2013**, *160*, C270−C276.

(19) Hosseinpour, S.; Hedberg, J.; Baldelli, S.; Leygraf, C.; Johnson, M. Initial Oxidation of Alkanethiol-Covered Copper Studied by Vibrational Sum Frequency Spectroscopy. *J. Phys. Chem. C* **2011**, *115*, 23871−23879.

(20) Laibinis, P. E.; Whitesides, G. M. Self-Assembled Monolayers of N-Alkanethiolates on Copper are Barrier Films that Protect the Metal against Oxidation by Air. *J. Am. Chem. Soc.* **1992**, *114*, 9022−9028.

(21) Nuzzo, R. G.; Allara, D. L. Adsorption of Bifunctional Organic Disulfides on Gold Surfaces. *J. Am. Chem. Soc.* **1983**, *105*, 4481−4483.

(22) Laibinis, P. E.; Whitesides, G. M.; Allara, D. L.; Tao, Y. T.; Parikh, A. N.; Nuzzo, R. G. Comparison of the Structures and Wetting Properties of Self-Assembled Monolayers of N-Alkanethiols on the Coinage Metal Surfaces, Copper, Silver, and Gold. *J. Am. Chem. Soc.* **1991**, *113*, 7152−7167.

(23) Fonder, G.; Cecchet, F.; Peremans, A.; Thiry, P. A.; Delhalle, J.; Mekhalif, Z. Conformational Order of N-Dodecanethiol and N-Dodecaneselenol Monolayers on Polycrystalline Copper Investigated by PM-IRRAS and SFG Spectroscopy. *Surf. Sci.* **2009**, *603*, 2276−2282.

(24) Santos, G. M.; Baldelli, S. Monitoring Localized Initial Atmospheric Corrosion of Alkanethiol-Covered Copper Using Sum Frequency Generation Imaging Microscopy: Relation between Monolayer Properties and Cu2O Formation. *J. Phys. Chem. C* **2013**, *117*, 17591−17602.

(25) Cimatu, K. A.; Baldelli, S. Chemical Microscopy of Surfaces by Sum Frequency Generation Imaging. *J. Phys. Chem. C* **2009**, *113*, 16575−16588.

(26) Cimatu, K.; Baldelli, S. Sum Frequency Generation Microscopy of Microcontact-Printed Mixed Self-Assembled Monolayers. *J. Phys. Chem. B* **2006**, *110*, 1807−1813.

(27) Wood, J. D.; Schmucker, S. W.; Lyons, A. S.; Pop, E.; Lyding, J. W. Effects of Polycrystalline Cu Substrate on Graphene Growth by Chemical Vapor Deposition. *Nano Lett.* **2011**, *11*, 4547−4554.

(28) Torchinsky, D. H.; Chu, H.; Qi, T.; Cao, G.; Hsieh, D. A Low Temperature Nonlinear Optical Rotational Anisotropy Spectrometer for the Determination of Crystallographic and Electronic Symmetries. *Rev. Sci. Instrum.* **2014**, *85*.

(29) Shen, Y. Surface Properties Probed by Second-Harmonic and Sum-Frequency Generation. *Nature* **1989**, *337*, 519−525.

DOI: 10.1021/acs.jpclett.5b00215
J. Phys. Chem. Lett. 2015, 6, 1454−1460

(30) Zhu, X.; Suhr, H.; Shen, Y. Surface Vibrational Spectroscopy by Infrared-Visible Sum Frequency Generation. *Phys. Rev. B* **1987**, *35*, 3047.
(31) Harris, A. L.; Chidsey, C. E. D.; Levinos, N. J.; Loiacono, D. N. Monolayer Vibrational Spectroscopy by Infrared-visible Sum Generation at Metal and Semiconductor Surfaces. *Chem. Phys. Lett.* **1987**, *141*, 350−356.
(32) Bain, C. D. Sum-Frequency Vibrational Spectroscopy of the Solid/Liquid Interface. *J. Chem. Soc. Faraday Trans.* **1995**, *91*, 1281−1296.
(33) Yeganeh, M. S.; Dougal, S. M.; Polizzotti, R. S.; Rabinowitz, P. Interfacialatomic-Structure of Self-Assembled Alkyl Thiol Monolayer Au(111)-A Sum-Frequency Generation Study. *Phys. Rev. Lett.* **1995**, *74*, 1811−1814.
(34) Harris, A.; Rothberg, L.; Dhar, L.; Levinos, N.; Dubois, L. Vibrational Energy Relaxation of a Polyatomic Adsorbate on a Metal Surface: Methyl Thiolate (CH3S) on Ag (111). *J. Chem. Phys.* **1991**, *94*, 2438−2448.
(35) Tom, H.; Aumiller, G. Observation of Rotational Anisotropy in the Second-Harmonic Generation from a Metal Surface. *Phys. Rev. B* **1986**, *33*, 8818.
(36) Sipe, J.; Moss, D.; Van Driel, H. Phenomenological Theory of Optical Second-and Third-Harmonic Generation from Cubic Centrosymmetric Crystals. *Phys. Rev. B* **1987**, *35*, 1129.
(37) Jennings, G. K.; Munro, J. C.; Yong, T.-H.; Laibinis, P. E. Effect of Chain Length on the Protection of Copper by N-Alkanethiols. *Langmuir* **1998**, *14*, 6130−6139.
(38) Malyk, S.; Shalhout, F. Y.; O'Leary, L. E.; Lewis, N. S.; Benderskii, A. V. Vibrational Sum Frequency Spectroscopic Investigation of the Azimuthal Anisotropy and Rotational Dynamics of Methyl-Terminated Silicon (111) Surfaces. *J. Phys. Chem. C* **2013**, *117*, 935−944.
(39) Wei, X.; Zhuang, X.; Hong, S.-C.; Goto, T.; Shen, Y. R. Sum-Frequency Vibrational Spectroscopic Study of a Rubbed Polymer Surface. *Phys. Rev. Lett.* **1999**, *82*, 4256−4259.
(40) Hirose, C.; Yamamoto, H.; Akamatsu, N.; Domen, K. Orientation Analysis by Simulation of Vibrational Sum Frequency Generation Spectrum: CH Stretching Bands of the Methyl Group. *J. Phys. Chem.* **1993**, *97*, 10064−10069.
(41) Parikh, A. N.; Allara, D. L. Quantitative Determination of Molecular Structure in Multilayered Thin Films of Biaxial and Lower Symmetry from Photo Spectroscopies.1.Reflection Infrared Vibrational Spectroscopy. *J. Chem. Phys.* **1992**, *96*, 927−945.
(42) Allara, D. L.; Swalen, J. D. An Infrared Reflection Spectroscopy Study of Oriented Cadmium Arachidate Monolayer Films on Evaporated Silver. *J. Phys. Chem.* **1982**, *86*, 2700−2704.
(43) Wang, H.-F.; Gan, W.; Lu, R.; Rao, Y.; Wu, B.-H. Quantitative Spectral and Orientational Analysis in Surface Sum Frequency Generation Vibrational Spectroscopy (SFG-VS). *Int. Rev. Phys. Chem.* **2005**, *24*, 191−256.
(44) Camillone, N.; Chidsey, C. E. D.; Liu, G.; Scoles, G. Substrate Dependence of the Surface-Structure and Chain Packing of Docosyl Mercaptan Self-Assembled on the (111), (110), and (100) Faces of Single-Crystal Gold. *J. Chem. Phys.* **1993**, *98*, 4234−4245.
(45) Love, J. C.; Estroff, L. A.; Kriebel, J. K.; Nuzzo, R. G.; Whitesides, G. M. Self-Assembled Monolayers of Thiolates on Metals as a Form of Nanotechnology. *Chem. Rev.* **2005**, *105*, 1103−1169.
(46) Poirier, G. E.; Tarlov, M. J. The C(4 × 2) Superlattice of N-Alkanethiol Monolayers Self-Assembled an Au(111). *Langmuir* **1994**, *10*, 2853−2856.
(47) Smith, R. K.; Lewis, P. A.; Weiss, P. S. Patterning Self-Assembled Monolayers. *Prog. Surf. Sci.* **2004**, *75*, 1−68.
(48) Zhuang, X.; Miranda, P. B.; Kim, D.; Shen, Y. R. Mapping Molecular Orientation and Conformation at Interfaces by Surface Nonlinear Optics. *Phys. Rev. B* **1999**, *59*, 12632−12640.

DOI: 10.1021/acs.jpclett.5b00215
J. Phys. Chem. Lett. 2015, 6, 1454−1460